Energy & Environmental Science

PAPER

View Article Online
View Journal | View Issue

Cite this: *Energy Environ. Sci.*, 2019, **12**, 1008

Energy scavenging from ultra-low temperature gradients†

Ravi Anant Kishore, *[a] Brenton Davis,[a] Jake Greathouse,[a] Austin Hannon,[a] David Emery Kennedy,[a] Alec Millar,[a] Daniel Mittel,[a] Amin Nozariasbmarz,[b] Min Gyu Kang,[a] Han Byul Kang,[a] Mohan Sanghadasa[c] and Shashank Priya *[ab]

Received 20th October 2018,
Accepted 21st January 2019

DOI: 10.1039/c8ee03084g

rsc.li/ees

Thermal energy harvesting from natural resources and waste heat is becoming critical due to ever-increasing environmental concerns. However, so far, available thermal energy harvesting technologies have only been able to generate electricity from large temperature gradients. Here, we report a fundamental breakthrough in low-grade thermal energy harvesting and demonstrate a device based on the thermomagnetic effect that uses ambient conditions as the heat sink and operates from a heat source at temperatures as low as 24 °C. This concept can convert temperature gradients as low as 2 °C into electricity while operating near room temperature. The device is found to exhibit a power density (power per unit volume of active material) of 105 μW cm^{-3} at a temperature difference of 2 °C, which increases to 465 μW cm^{-3} at a temperature difference of 10 °C. The power density increases by 2.5 times in the presence of wind with a speed of 2.0 m s^{-1}. This advancement in thermal energy harvesting technology will have a transformative effect on renewable energy generation and in reducing global warming.

Broader context

Low-grade heat, either in the form of waste heat from industrial processes or naturally available sources such as hot springs, represents an extremely promising source of renewable energy. Thorough analysis of available low-grade heat has revealed that recovering just 1.5% of it can generate more electricity than currently produced by wind, solar, and tidal combined. A cost-effective method for recovering low-grade heat will have a transformative impact on the overall energy scenario. Current thermal energy harvesting technologies such as the organic Rankine cycle, the Kalina cycle, Stirling engines and thermoelectric generators have very poor efficiency when the hot-side temperature is less than 100 °C, making them economically unviable for low-grade heat recovery. Here we report a fundamental breakthrough in demonstrating an ultra-low thermal gradient energy recovery mechanism, termed as PoWER (Power from Wasted Energy Recovery). PoWER devices use ambient conditions as a heat sink and operate from a heat source at temperatures as low as 24 °C. The PoWER devices demonstrated here are capable of generating electricity by utilizing rejected heat from a laptop, a sewer grill, and an outdoor metal bench exposed to sunlight. The device is found to exhibit a power density of 465 μW cm^{-3} at a heat source temperature of 32 °C, which increases by two to three times in the presence of wind with a speed of 1.5–2.0 m s^{-1}.

Introduction

Annually, 340 exajoules (1 EJ = 10^{18} J) of energy out of 474 EJ of energy generated from various renewable and non-renewable energy resources is rejected as waste heat.[1] Low-grade waste heat with a temperature less than 100 °C constitutes more than 60% of the total waste heat.[1] In addition to the waste heat available from various industrial and household sources, there are natural thermal energy sources, such as hot springs, geothermal heat, and solar heat, whose temperature varies from room temperature to the evaporation temperature of water. Unarguably, low-grade heat, either in the form of waste heat or natural sources, represents an extremely promising source of renewable energy, as it is commonly available in our local surroundings. The Carnot efficiency of a low-grade heat recovery engine operating between 100 °C and ambient temperature at 25 °C can be calculated to be about 20%. This infers that a cost-effective method to recover low-grade heat would have a transformative impact on the overall energy scenario.

[a] *Center for Energy Harvesting Materials and Systems (CEHMS), Virginia Tech, Blacksburg, VA 24061, USA. E-mail: ravi86@vt.edu*
[b] *Department of Materials Science and Engineering, Pennsylvania State University, University Park, PA 16802, USA. E-mail: sup103@psu.edu*
[c] *Aviation and Missile Research, Development, and Engineering Center, US Army RDECOM, Redstone Arsenal, AL 35898, USA*

† Electronic supplementary information (ESI) available. See DOI: 10.1039/c8ee03084g

Traditionally, binary organic Rankine cycle[2,3] and Kalina cycle[4] based power plants have been used for electricity generation from medium-temperature (100–220 °C) heat resources. However, as the available temperature difference is reduced, the performance of these power plants deteriorates and at temperatures below 100 °C, the cycle efficiency reduces to 5–9%.[5] Further, with low-temperature sources, traditional heat engines require large heat exchangers,[6] which imposes additional space and material cost, making them economically unviable. The Stirling engine is another popular option for low-grade heat recovery. Small Stirling engines have been reported to start at a temperature difference as low as 0.5 °C[7] and generate power on the order of 0.3–2.5 mW when the temperature difference is 6.5–19 °C.[8,9] Stirling engines, however, employ a gas as the working fluid which requires a large storage volume and imposes several operational challenges due to diffusion and leakage.[10] A better alternative to capture low-grade heat is through thermal energy harvesting. Energy harvesting provides a methodology for generating electricity from environmental energy sources that are freely available. Energy harvesting devices comprising solar cells[11,12] and vibration harvesters[13–15] have been widely pursued in the literature and recently there has been a surge in developing thermal energy harvesters. Various approaches based upon thermoelectrics, pyroelectrics, thermal polymer-muscles, and shape memory alloys are being considered.[16] Thermoelectric generators (TEGs) utilizing the Seebeck effect represent one of the most popular heat recovery technologies.[17,18] Although recent studies have reported a TEG efficiency close to 10% when the temperature gradient is large (more than 500 °C),[19,20] the efficiency of commercially available TEGs is still quite low, not more than a few percent.[21] The efficiency of TEGs, and indeed all heat engines, deteriorates as the thermal gradient decreases, which makes them impractical for low-grade heat recovery (hot-side temperatures lower than 100 °C). This is related to the peak behaviour of the figure-of-merit for thermoelectric materials, which in most cases occurs above 100 °C. Shape memory alloy (SMA) based generators have been recently proposed as an alternative for low temperature heat recovery.[22,23] SMA engines rely on a thermoelastic effect, where an SMA element undergoes a reversible phase transformation from a martensite to an austenite phase, generating cyclic strain, which is used to generate torque that drives an electromagnetic generator. SMA engines have been reported to operate in the temperature range of 60–80 °C and found to exhibit 187 mW of electrical power from a device with dimensions 1850 mm × 550 mm × 500 mm, resulting in a power density of 0.4 W m^{-3}.[22] Pyroelectrics and thermal polymer-muscles have been projected to exhibit high power density (1.08 MW m^{-3} of the PVDF film under a temperature change of 80 °C for a pyroelectric generator[24] and 18.1 kW m^{-3} of the coiled muscle across a temperature fluctuation of 70 °C for the polymer-muscle powered tensile energy generator).[25] Although both these technologies are being targeted for waste heat recovery, their requirement of cyclic temperature variation limits their deployment. In addition, high power density in these cases is accompanied by very low overall power output for a given volume, which makes integration or operation such as recharging of batteries quite difficult.

A fundamentally different approach for harnessing low-grade thermal energy and converting it into mechanical or electrical energy is possible using the thermomagnetic effect. The concept of a thermomagnetic generator was first proposed in the late 19th century,[26–29] but this promising technology was not implemented due to lack of a suitable ferromagnetic material. Conventional ferromagnetic materials such as iron, cobalt, and nickel have Curie temperatures above 350 °C, which presents several implementation challenges. Gadolinium (Gd), having a low Curie temperature of 22 °C, has been proposed as a suitable thermomagnetic material for a thermomagnetic generator.[30] The ferromagnetic to paramagnetic transition normally occurs in a narrow temperature range; therefore, in comparison with conventional ferromagnetic materials, Gd is expected to exhibit a higher Carnot efficiency for the same value of ΔT (*i.e.* for a fixed temperature difference, ΔT, the Carnot efficiency $\Delta T/T_h$ increases with a decrease in the hot reservoir temperature T_h).[31] Analytical studies[32–35] have revealed that Gd based thermomagnetic heat engines can provide efficiencies approaching the Carnot efficiency; however, no known experimental work has been performed to prove this possibility which indicates the challenges associated with translating the theory into practice. Factors such as material availability, manufacturability, actual operating conditions, environmental effects, and cost are just a few of the challenges that often lead to violation of assumptions made in analytical calculations. A few recent studies[36–40] have reported Gd based thermomagnetic harvesters, however, these devices often require a heat sink below 0 °C, which questions the economic feasibility of these low power density devices.

In this study, we demonstrate a unique ultra-low thermal gradient energy recovery mechanism, called PoWER (Power from Waste Energy Recovery), with ambient conditions acting as the heat sink. The PoWER device does not require an external heat sink, bulky fins or thermal fluid circulation. A small size, room temperature operation, and a cost-effective configuration make our device highly suitable for power generation in a wide range of applications including recharging a battery for the internet-of-things, self-powered temperature sensing, water quality monitoring, occupancy detection sensors, and power generation. A PoWER device utilizes the thermomagnetic effect, where a cyclic variation in temperature across the Curie temperature of a ferromagnetic material in the presence of an external magnetic field results in a cyclic change in magnetization, which is used to create mechanical work. A home built two-rotor one-stator axial flux electric generator is connected to a thermomagnetic engine to convert mechanical power into electricity.

Results and discussion

Material, working principle, and device design

The thermomagnetic material employed in this study is Gd as its Curie temperature is close to room temperature. Gd possess

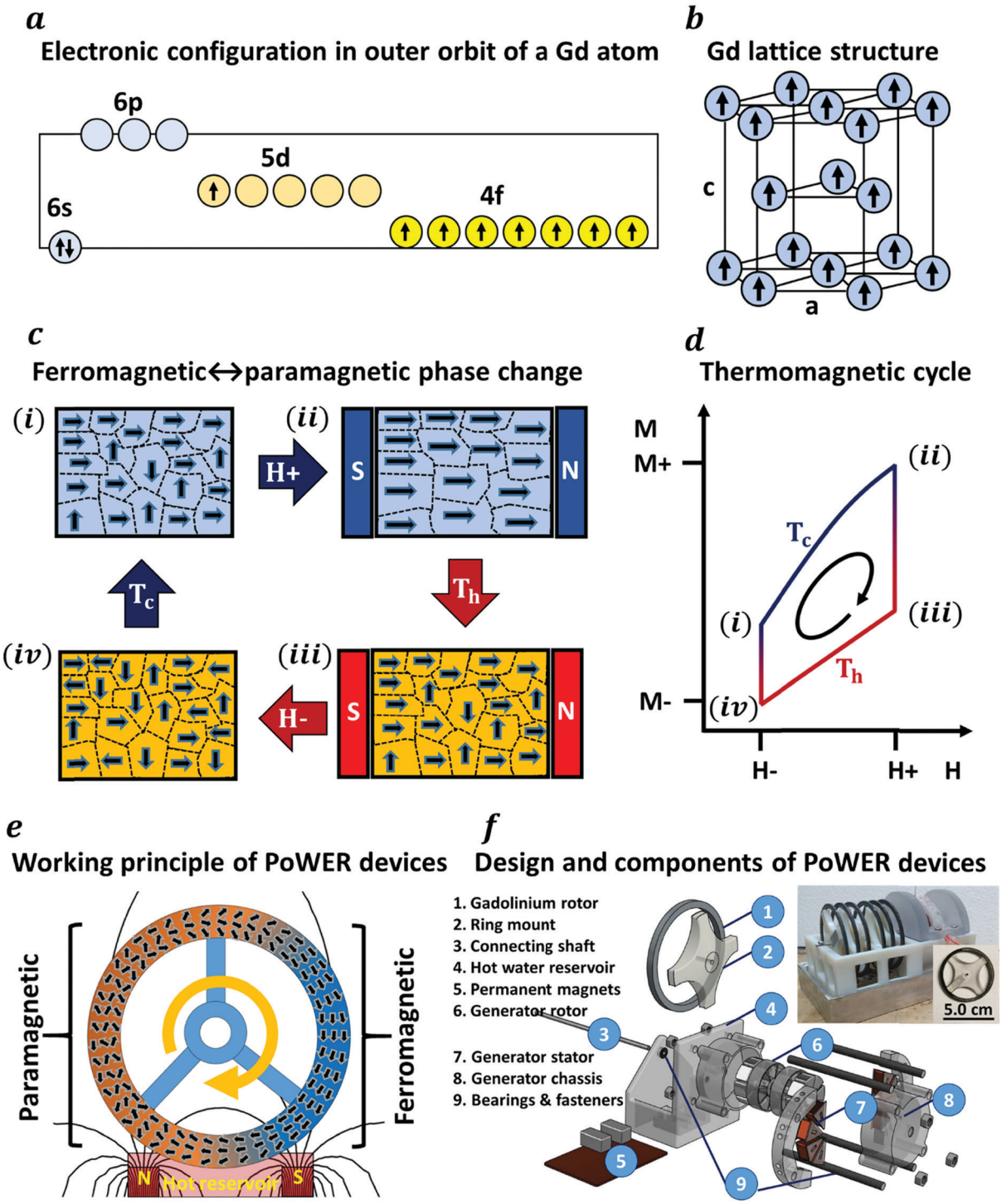

Fig. 1 Harvesting ultra-low grade thermal energy from the surroundings. (a) The electronic configuration in the outer orbit of a neutral Gadolinium (Gd) atom. The seven unpaired electrons in the 4f subshell account for the large magnetic moment of Gd. (b) The hexagonal close-packed (hcp) structure of a Gd crystal. From the spin reorientation temperature (−41 °C) to the Curie temperature (22 °C), the magnetic moments are aligned along the hexagonal axis (*c*-direction). (c) The thermal energy harvesting utilizing a thermomagnetic material that can be employed to obtain magnetic work. (d) The thermomagnetic cycle, where a Gd sample undergoes a second-order paramagnetic ↔ ferromagnetic phase transformation in a cyclic manner. (e) The working principle of the proposed ultra-low grade thermal energy recovery mechanism, PoWER (Power from Waste Energy Recovery). Cyclic heating and cooling causes magnetic domains to orient and disorient, resulting in time-varying magnetization and an unbalanced magnetic torque on the rotor. (f) The design architecture and key components of the PoWER device. A prototype of the PoWER device with six rotors is shown in the inset.

a large magnetic moment below its Curie temperature because of its electronic configuration, [Xe] $4f^7$ $5d^1$ $6s^2$. Fig. 1a depicts the electronic configuration in the outer orbit of a neutral Gd atom.[41] The seven unpaired electrons in its 4f subshell account

for a total angular momentum (spin angular momentum, S, and orbital angular momentum, L) of $J = L + S = 7/2$.[42] The saturation magnetic moment of Gd has been reported to be 7.55 μ_B. An additional 0.55 μ_B moment is attributed to conduction electron polarization.[43] Gd crystallizes in the hexagonal close-packed structure and from the spin reorientation temperature (−41 °C) to the Curie temperature (22 °C), the magnetic moments are aligned along the hexagonal axis (c-direction), as shown in Fig. 1b.[44]

Gd undergoes a second-order paramagnetic ↔ ferromagnetic phase transformation, which can be utilized to obtain magnetic work using the thermomagnetic cycle shown in Fig. 1c and d. Phase i, shown in Fig. 1c and d, denotes the state of spontaneous magnetization where a Gd sample is below its Curie temperature and in zero external magnetic field. When an external magnetic field H+ is applied, the magnetic moments orient in the direction of the magnetic field, leading to an increase in the size of magnetic domains (shown as state ii). The Gd sample is then heated above the Curie temperature while the external magnetic field is kept constant. The magnetization reduces due to thermal agitation, which is indicated by state iii. When the external magnetic field is removed, the magnetic moments fully disorient, leading to near zero magnetization in the Gd sample (state iv). Lastly, the Gd sample is cooled to its initial temperature and state i is restored. It is important to note that when the temperature across a ferromagnetic material is changed, the material needs some time to establish a new equilibrium magnetization. This characteristic time is termed as the spin–lattice relaxation time and it measures the strength of the coupling between the spin system and the lattice. In the case of Gd, the characteristic time for establishing thermal equilibrium between the lattice and the spin system has been reported to be on the order of picoseconds.[45] Since the magnetic response of Gd is quite fast, the overall frequency of a Gd-based thermomagnetic cycle is primarily controlled by the frequency at which thermal cycling occurs.

Fig. 1e demonstrates the working principle of the proposed PoWER mechanism based on the thermomagnetic effect. The PoWER device consists of ring-shaped Gd rotors, permanent magnets, and an electric generator. Fig. 1f shows an assembled PoWER device having six rotors. Warm water (T_h = 24–50 °C) is used as the hot reservoir to heat a small section of the Gd rotor above its Curie temperature. The external magnetic field is created using the two permanent magnets located below the rotors, as shown in Fig. 1f. This two-magnet configuration helps the PoWER device to achieve a higher rotor speed and magnetic torque as compared to the one-magnet configuration (please refer to the ESI,† Fig. S6 for more discussion). The portion of the rotor in contact with the warm water gains heat and a hot spot is created. When the temperature rises above the Curie temperature, the rotor locally undergoes the second-order ferromagnetic to paramagnetic phase transformation, causing the magnetic domains to disorient due to thermal agitation. This drastically reduces the magnetic interaction between the hot spot and the permanent magnet. Since the remaining part of the rotor is still cold and in the ferromagnetic phase, the permanent magnet attracts the cooler portion resulting in a net torque on the rotor, which causes it to rotate. As rotation occurs, the hot portion cools down by dissipating heat to the ambient air and the magnetic domains regain their orientation. Eventually, a new hot spot is created, and the rotation continues as long as there is a heat source. An axial flux electric generator is connected to the rotor in order to harvest this rotational motion and generate electricity. The details of the device fabrication are provided in the Experimental section. A detailed discussion on the thermomagnetic effect, the thermomagnetic material, and the calculation for the specific work and the efficiency of the thermomagnetic cycle are provided in the ESI.†

Thermomagnetic cycle in the PoWER rotor

Fig. 2a and b illustrate the magnetic field distribution and temperature distribution along the rotor's surface of the PoWER device. The contours were obtained using COMSOL Multiphysics (version 5.3). As shown in Fig. 2a, the magnetic flux density varies between ∼0 T and 0.22 T. This infers that during each rotation, a portion of the rotor experiences a magnetic cycle in the range 0–0.22 T. Fig. 2b shows the temperature contour. It was noted that the actual temperature distribution is dependent on the rotor's angular speed; however, the extreme values for the rotor temperature always lie between the water and ambient temperature. Fig. 2c depicts the magnetization *versus* magnetic field (M–H) plots for Gd, obtained using the quantum design physical property measurement system (PPMS). Using eqn (S1), ESI,† and integrating around the thermomagnetic cycle, the specific magnetic work per thermomagnetic cycle occurring between 0 and 0.22 T and 22 and 40 °C can be calculated to be ∼3.5 J kg^{-1}. In Fig. 2c, it is also important to note that the isotherms are very close when the temperature is greater than 40 °C. This implies that the performance of PoWER devices cannot be increased substantially by increasing the hot-side temperature beyond 40 °C. Fig. 2d shows the specific heat *versus* temperature (C_H–T) plots for Gd measured using differential scanning calorimetry (DSC). The shaded region depicts the heat flow when the temperature cycle occurs between 22 °C and 40 °C. Using eqn (S8), ESI,† the efficiency of the thermomagnetic cycle was calculated to be ∼0.1%. Since the specific work output per thermomagnetic cycle increases with an increase in the applied magnetic field, it is estimated that when the applied magnetic field is 1.0 T, the efficiency can be increased to 0.6%. Please note that the Carnot efficiency of a heat engine working between T_c = 22 °C and T_h = 40 °C is 5.8%. This illustrates that thermomagnetic cycle based PoWER devices have the potential to operate up to a 10% Carnot efficiency.

Performance characteristics of the PoWER devices

Fig. 3a depicts the electrical power produced by the PoWER device having a single rotor of dimensions of 50.5 mm (outer diameter, OD) × 44.5 (inner diameter, ID) × 1.5 mm (thickness),

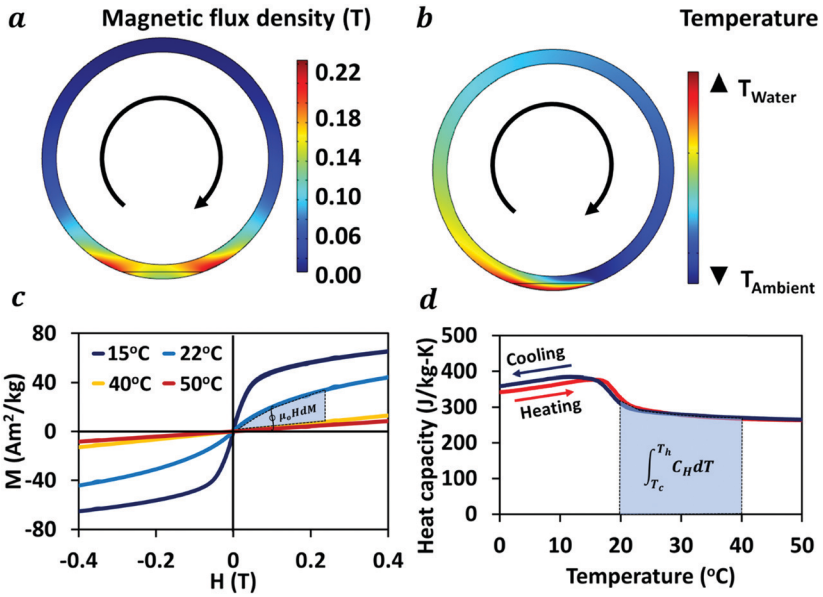

Fig. 2 Thermomagnetic cycle in the PoWER rotor. (a) The magnetic flux density distribution along the surface of the PoWER rotor. (b) The temperature contour showing the temperature distribution along the surface of the PoWER rotor. The actual temperature depends on the angular speed of the PoWER rotor. (c) Isothermal magnetization–magnetic field (M–H) curves of Gd. The shaded region illustrates the specific work. Isotherms are very close at high temperature, indicating minimal increase in specific work above 40 °C. (b) Heat capacity *versus* temperature of the Gd sample used in the PoWER devices. The shaded region indicates the heat flow during the thermomagnetic cycle.

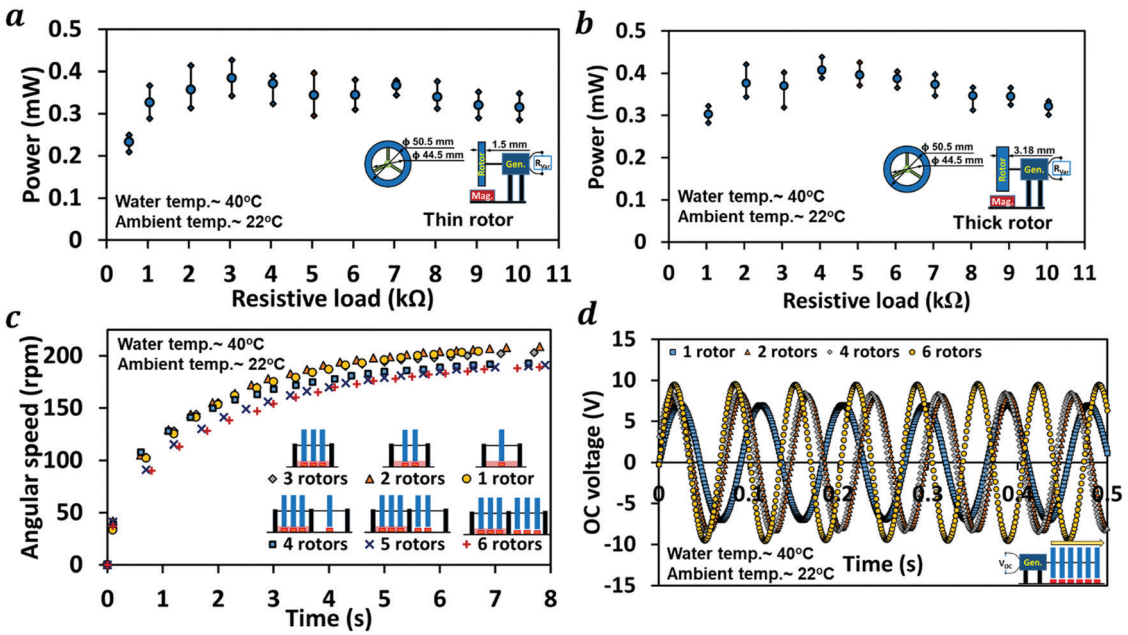

Fig. 3 Electrical power produced by PoWER devices as a function of resistive load at a water temperature of 40 °C and ambient temperature of 22 °C. (a) The maximum, minimum, and average electrical power output of the PoWER device having a thin rotor of dimensions 50.5 mm (OD) × 44.5 (ID) × 1.5 mm (thickness). (b) The maximum, minimum, and average electrical power output of the PoWER device having a thick rotor of dimensions 50.5 mm (OD) × 44.5 (ID) × 3.18 mm (thickness). The thicker rotor (3.18 mm thickness) produces a 6% higher power than the thinner one (1.5 mm thickness). (c) The angular speed progression of the PoWER rotor from the time it starts until it reaches the steady state. The number of rotors does not significantly affect the steady state angular speed and the angular acceleration, indicating the thermomagnetic cycles of different rotors are mutually independent and the magnetic torque can be increased by increasing the number of rotors. (d) Open circuit (OC) voltage obtained for different PoWER devices having one, two, four, and six rotors, respectively. The OC voltage has a frequency of 12.7 Hz, 13.1 Hz, 13.5 Hz, and 14.3 Hz, respectively, and an amplitude above 1.0 V to minimize losses during rectification.

when the warm water temperature is maintained at 40 °C and the ambient temperature is at 22 °C. The maximum, minimum, and average electrical power obtained during experiments are shown in Fig. 3a at different resistive loads. A maximum average

electrical power of 0.385 mW was obtained at an optimal resistive load of 3 kΩ. Fig. 3b depicts the electrical power produced by the PoWER device with a rotor of the same OD and ID as discussed earlier but a different thickness of 3.18 mm. A maximum average electrical power of 0.407 mW was observed at an optimal resistive load of 4 kΩ. This indicates that there is not much gain in power by increasing the rotor thickness, but this is an important result that illustrates the role of the coupling between the thermal transport and the physical behavior of the material. Gd, the thermomagnetic material used for the rotor, has thermal conductivity of 9.5 W m^{-1} K^{-1}.[46] Analytical calculations show that heat propagates just a few microns inside the rotor when it is operating at the optimal load in the steady state condition. The thermal cycling, therefore, occurs only near the outer surface, making the additional thickness unnecessary. Fig. S4, ESI,† depicts the effect of the size of the rotor on the performance of the PoWER devices. It can be noted that increasing the size of the rotor has a positive influence on the generated electrical power due to the increased thermal gradient. Therefore, in the remainder of the paper, results for a rotor of dimensions 50.0 mm (OD) × 44.5 (ID) × 1.5 mm (thickness) will be presented. Fig. 3c depicts the angular speed progression of the PoWER rotor (not connected to a generator) from the time it starts and until it reaches the steady state. It can be noted that increasing the number of rotors does not significantly affect the steady state angular speed and the angular acceleration; although the maximum angular speed slightly decreased after three rotors due to additional damping. This indicates that the thermomagnetic cycles occurring in different rotors are mutually independent of each other and the magnetic torque can be increased by increasing the number of rotors. Fig. 3d shows the open circuit (OC) voltage produced by the PoWER devices having a variable number of rotors (one to six) connected simultaneously to a single generator shaft. In order to account for the increased magnetic torque due to multiple rotors, a bigger electric generator compared to the generator used for the PoWER device with a single rotor was implemented. The details of generator characteristics are provided in the ESI.† The EMF frequency of the electric generator is related to the shaft rpm by the relation: $f = np/120$, where n is the shaft rpm and p denotes the number of magnetic pole pairs used in the electric generator. The steady state, no-load rpm for PoWER devices having one, two, four, and six rotors was found to be 191, 196, 202, and 215, respectively, at a water temperature of 40 °C. This corresponds to an operational frequency of 12.7 Hz, 13.1 Hz, 13.5 Hz, and 14.3 Hz, respectively, where OC voltages were measured. The output voltage amplitude above 1.0 V ensures minimal losses during AC to DC rectification.

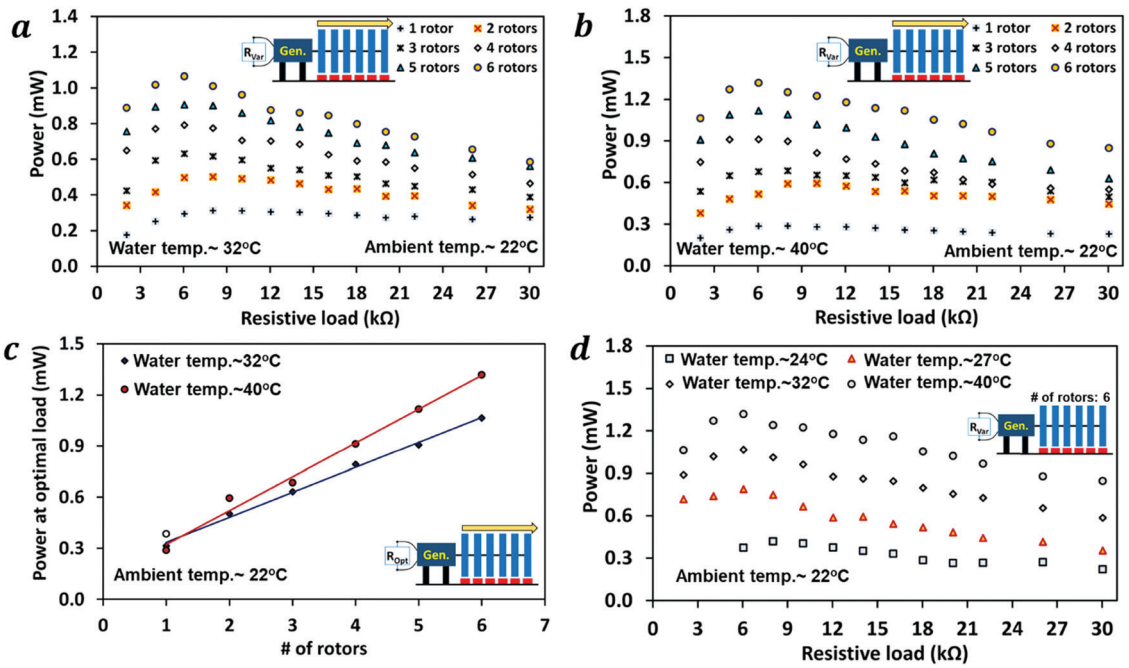

Fig. 4 Electrical power produced by PoWER devices having multiple rotors as a function of resistive load. (a) The average electrical power produced by the PoWER device having multiple rotors connected simultaneously to a single generator shaft. At a water temperature of 32 °C, the electrical power at the optimal resistive load increases from 0.31 mW to 1.10 mW by increasing the number of rotors from one to six. (b) The average electrical power produced by the PoWER device having multiple rotors at 40 °C. The electrical power at the optimal resistive load increases from 0.30 mW to 1.30 mW by increasing the number of rotors from one to six. (c) The optimal power of the PoWER devices *versus* number of rotors. The hollow circle shows the optimal power of the PoWER device with a single rotor attached to small generator. The optimal power increases almost linearly with the increase in the number of rotors, emphasizing the fact that the device is scalable and the power per unit volume of the device can be increased substantially by increasing the number of rotors. (d) The average power of the PoWER device with six rotors at different hot-water temperatures. The PoWER device produces an optimal power of 0.42 mW at a water temperature of 24 °C (a temperature difference of 2 °C) and 0.79 mW at a water temperature of 27 °C (a temperature difference of 5 °C).

Fig. 4a and b depict the electrical power produced by the PoWER device having multiple rotors connected simultaneously to a single generator shaft. It can be observed that at a hot water temperature of 32 °C, the electrical power at the optimal resistive load increases from 0.31 mW to 1.10 mW by increasing the number of rotors from one to six. Likewise, at a hot water temperature of 40 °C, the optimal electrical power increases from 0.30 mW to 1.30 mW by increasing the number of rotors from one to six. As indicated in Fig. 4c, the optimal power of the PoWER devices increases almost linearly with the increase in the number of rotors. Fig. 4d shows the output power of the PoWER device with six rotors at different hot-water temperatures. It is interesting to note that the PoWER device operates at a water temperature of 24 °C (*i.e.* a temperature difference of just 2 °C) and produces an electrical power of 0.42 mW, which increases to 0.79 mW at a water temperature of 27 °C (a temperature difference of 5 °C), 1.10 mW at a water temperature of 32 °C (a temperature difference of 10 °C), and 1.30 mW at a water temperature of 40 °C (a temperature difference of 18 °C). More detailed discussion on the scalability of PoWER devices is provided in the ESI.†

PoWER device performance as a function of temperature

Fig. 5a and b demonstrate the performance of the PoWER device with three rotors during a temperature sweep experiment. As indicated in Fig. 5a, the rotor rpm initially increases with an increase in water temperature, but then saturates at ~50 °C. This happens because of the counteractive effects between thermal and magnetic physics. The convective heat transfer coefficient is proportional to the relative speed between the ambient air and the rotating rotor, whereas the magnetic force is proportional to the lowest temperature achieved by the rotor. When the water temperature is low, the rotor tends to move faster as a higher rpm helps the hot spot in the rotor to cool faster and thus amplifies the paramagnetic to ferromagnetic phase transformation. However, when the temperature of the hot spot is much above the Curie point, the high rpm of the rotor does not allow it to cool below the Curie temperature, thereby restricting the paramagnetic to ferromagnetic phase transition. Therefore, when the water temperature is low (25–30 °C), the rotor speeds up, however when the water temperature rises to a threshold value of ~50 °C, the rotor attains a constant speed of around 200 rpm. A similar trend was observed for the power output (Fig. 5b). The electrical power of the PoWER device first increases with an increase in temperature, reaches a maximum value at 35–45 °C, and then decreases slowly. This can be explained by invoking the *M–H* diagram shown in Fig. 2c. Since the isotherms are close at high temperature, the shaded area does not increase substantially beyond 40 °C, thereby causing a very small increase in the power generated by PoWER devices. The temperature sweep experiments were repeated on the PoWER device with two rotors, which are shown in Fig. S2 and S3 in the ESI.†

Effect of wind on the performance of PoWER devices

Fig. 6a–d quantify the effect of wind (forced cooling) on the performance of the PoWER devices. The optimal power of the PoWER device with three rotors increases from 0.69 mW under no wind conditions to 1.5 mW under a wind speed of 1.5 m s^{-1} and to 1.8 mW under a wind speed of 2.0 m s^{-1}. Likewise, the optimal power of a PoWER device with six rotors increases from 1.3 mW under no wind conditions to 2.3 mW under a wind

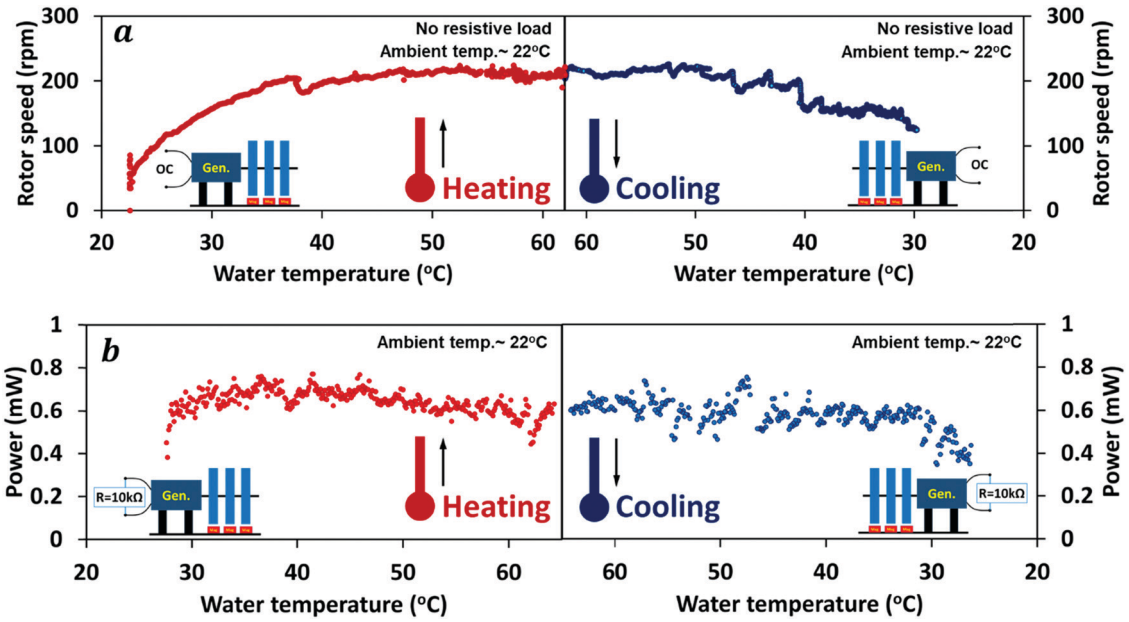

Fig. 5 Temperature sweep experiment for the PoWER device with three rotors. (a) Variation in the rotor rpm with an increase and a decrease in the water temperature. When the water temperature is very low, the rotor speeds up, but as the water temperature rises above a threshold value, the rotor achieves nearly a constant speed. (b) Variation in the power output of the PoWER device with an increase and a decrease in the water temperature. The electrical output first increases with an increase in temperature, reaches a maximum value at 35–45 °C, and then decreases slowly.

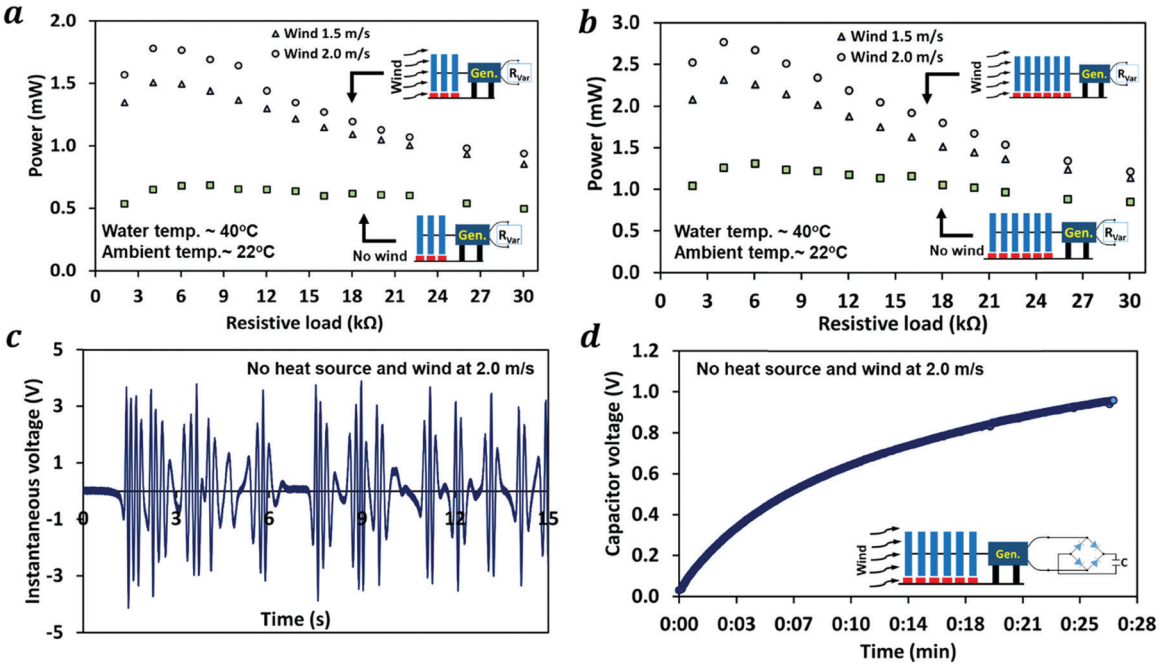

Fig. 6 Effect of wind (forced cooling) on the performance of PoWER devices. (a) Performance of the PoWER device with three rotors at wind speeds of 1.5 m s^{-1} and 2.0 m s^{-1}. The optimal power of the PoWER device with three rotors increases from 0.69 mW in no wind conditions to 1.5 mW in wind conditions of 1.5 m s^{-1} and 1.8 mW in wind conditions of 2.0 m s^{-1}. (b) Performance of the PoWER device with six rotors at wind speeds of 1.5 m s^{-1} and 2.0 m s^{-1}. The optimal power of a PoWER device with six rotors increases from 1.3 mW in no wind conditions to 2.3 mW under a wind speed of 1.5 m s^{-1} and 2.8 mW under a wind speed of 2.0 m s^{-1}. (c) Voltage generated by the PoWER device when there is no heat source but a wind speed of 2.0 m s^{-1}. (d) The voltage across the two terminals of a 2.5 V 0.2 F capacitor being charged using the power produced by the PoWER device under no heat source and wind of 2.0 m s^{-1}.

speed of 1.5 m s^{-1} and to 2.8 mW under a wind speed of 2.0 m s^{-1}. Fig. 6c depicts interesting behavior from a PoWER device. It was observed that the PoWER device is capable of operating with no heat source when there is light wind. As shown in the ESI,† Video V1, the PoWER device does not self-start when there is no heat source; however, once it is started manually, the rotor maintains oscillation. The chilling effect produced by the wind evaporates water drawn onto the exposed portion of the rotor during oscillation. This causes the exposed portion of the rotor to cool slightly below room temperature, thereby creating a thermal gradient in the rotor. The continuous rewetting of the Gd rotor and evaporation by the wind allows the PoWER device to maintain oscillation. The axial AC generator, which is attached to the rotor, captures this oscillation and generates electricity. Fig. 6d shows the voltage across the two terminals of a 2.5 V 0.2 F capacitor, which was charged using the power produced by the PoWER device under wind of 2.0 m s^{-1} and no heat source.

Power density of the PoWER devices

Fig. 7 shows the power density (power per unit volume of Gd) of the PoWER devices at two different temperatures. At a fixed temperature difference of 10 °C, a power density of 467 μW cm^{-3} is obtained with a single rotor. As the number of rotors is increased, the power density slowly decreases and almost saturates at 265 μW cm^{-3} for six rotors. Likewise, at a fixed temperature difference of 18 °C, a power density of 442 μW cm^{-3} is obtained with two rotors and as the number of rotors is increased, the power density decreases and it approximately saturates at 328 μW cm^{-3} for six rotors. The figure in the inset shows the power density for the PoWER device with six rotors under a varying temperature difference. The PoWER device with six rotors produces a power density of 105 μW cm^{-3} under a temperature difference of 2 °C, which increases to 328 μW cm^{-3} under a temperature difference of 18 °C.

There are a limited number of studies in the literature that quantify the experimental output power for a heat engine operating near room temperature under such low temperature gradients. Most of the thermomagnetic harvesters reported in

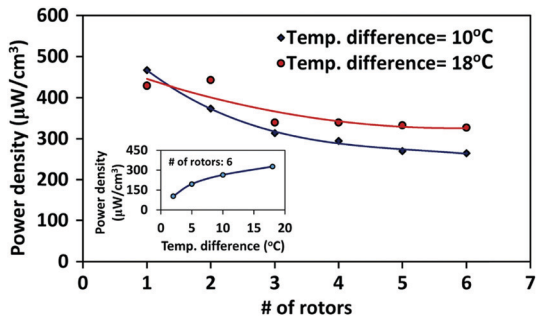

Fig. 7 Power density (power per unit volume of Gd) demonstrated by PoWER devices having various numbers of rotors. The figure in the inset shows the power density for the PoWER device with six rotors at different temperature differences.

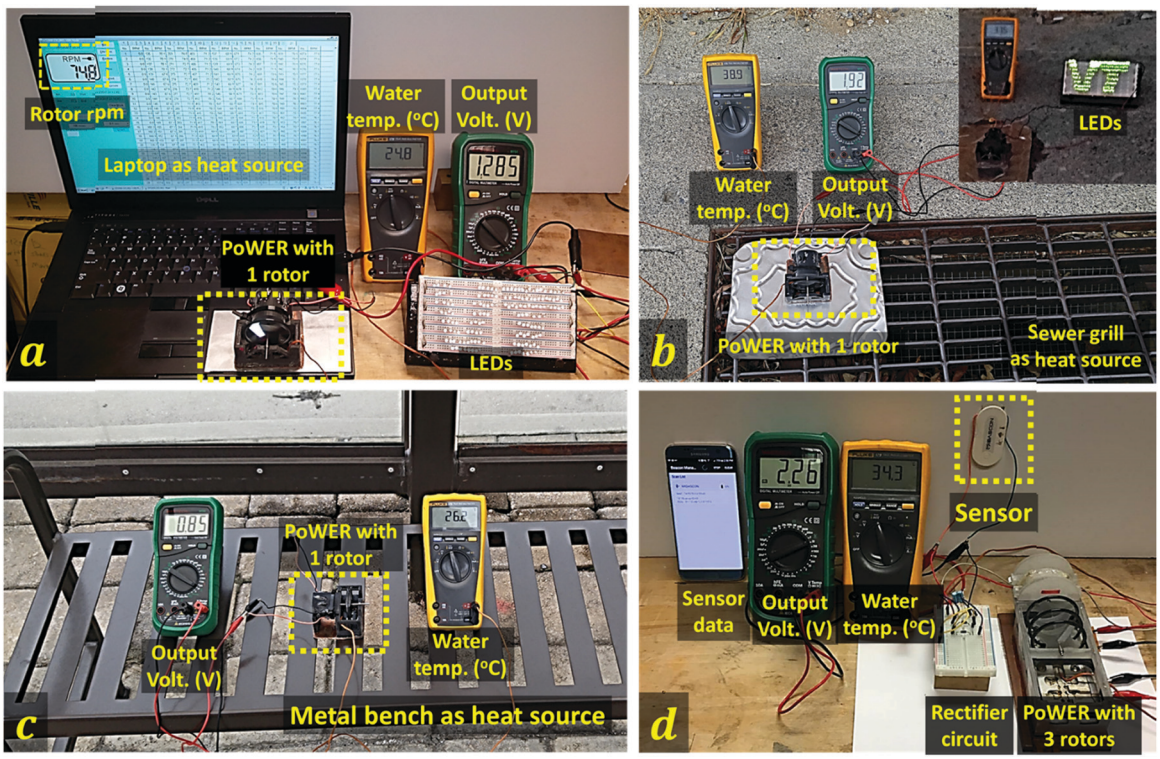

Fig. 8 Some real-world demonstrations. (a) A PoWER device with a single rotor kept on the surface of a laptop. Utilizing rejected heat from the laptop, the PoWER device can power several LEDs. (b) A PoWER device located on a sewer grill. The PoWER device generates electricity using the steam coming out of the sewage and drainage system. (c) A PoWER device with a single rotor is kept on a metal bench exposed to sunlight. The PoWER device can operate under a thermal gradient of just 1 °C between the heat source and the ambient air. (d) A MIDASCON sensor being powered by a PoWER device. The sensor measures temperature, humidity, and acceleration and transmits the data wirelessly using Bluetooth.

the literature are based on the linear oscillation of a thermomagnetic material attached to a spring–mass system. They also rely on the piezoelectric effect to generate electricity.[36–39,47] Based on the average power reported by Chen *et al.*,[38] the power density (power per unit volume of the thermomagnetic material) of such harvesters was estimated to be 0.0132 μW cm^{-3} at a temperature difference of 20 °C, which is lower by several orders of magnitude than the power density demonstrated by PoWER devices. It is also important to note that the current version of PoWER devices utilizes a commercial off-the-shelf non-optimized thermomagnetic material, Gd. There are several prototype thermomagnetic materials, such as GdSiGe alloys[48,49] and Heusler alloys,[50,51] that have been reported to exhibit a 2–10 times higher thermomagnetic effect than that of Gd. In addition, simulation results shown in the ESI† show that the performance of the PoWER devices can be increased by increasing the applied magnetic field. This implies that the power density of the PoWER devices can be improved several fold by performing material and system optimization in future studies. We believe PoWER will provide the foundation to launch a new generation of thermal energy harvesting devices.

Real-world demonstrations using PoWER devices

Fig. 8a–d demonstrate the deployment of PoWER devices for real-world applications. In Fig. 8a, the PoWER device with a single rotor was kept on the surface of a laptop. Gaining the heat dissipated by the laptop, the water temperature below the rotor rises to 25 °C, when the room temperature is at 22 °C. As shown in the ESI,† Video V2, under a temperature difference of just 3 °C, the PoWER device with a single rotor can be seen to light up several LEDs. Fig. 8b demonstrates the operation of the PoWER device when it is located on a sewer grill. The demonstration shown in the ESI,† Video V3, depicts that the PoWER device can be employed to generate electricity using rejected heat from the steam coming out of sewage and drainage systems from industrial and commercial establishments. In Fig. 8c, the PoWER device with a single rotor is kept on a metal bench, which is exposed to sunlight. Video V4, ESI,† shows the demonstration, where the PoWER device can be seen to operate under a thermal gradient of just 1 °C (the ambient temperature is 25.3 °C, whereas the water temperature is 26.3 °C). A PoWER device was also employed to continuously run a MIDASCON wireless sensor that senses temperature, humidity, and acceleration and transmits the data using Bluetooth, as shown in Fig. 8d and the ESI,† Video V5. These successful demonstrations clearly indicate that PoWER devices can harvest thermal energy from a variety of heat sources and can be used in a wide range of applications.

Conclusions

We report a fundamental breakthrough in demonstrating an ultra-low grade thermal energy recovery mechanism, termed as

PoWER (Power from Wasted Energy Recovery), based on the thermomagnetic effect. The PoWER device uses ambient conditions as the heat sink and is found to operate with a heat source at temperatures as low as 24 °C. The PoWER device is found to exhibit a power density (power per unit volume of Gd) of 105 μW cm^{-3} at a temperature difference of 2 °C, which increased to 465 μW cm^{-3} at a temperature difference of 10 °C. The power density increases by 2.5 times in the presence of light wind with a speed of 2.0 m s^{-1}. The PoWER device is also able to operate at zero thermal gradient when there is light wind.

Experimental

Fabrication of PoWER devices

In order to demonstrate the PoWER mechanism, we fabricated scaled versions of the PoWER device. The device consists of Gd ring shaped rotors of outer diameter (OD) 50.5 mm and inner diameter (ID) 44.5 mm, permanent magnets of size 12.7 mm × 6.35 mm × 6.35 mm, and an axial flux generator. Preliminary experiments reveal that two permanent magnets located below the rotor, as shown in Fig. 1f, provide the highest power (the effect of the number of permanent magnets on the performance of PoWER devices is discussed in the ESI†). Gd sheets (purity: 99.9%) of 200 mm × 400 mm × 1.5 mm purchased from Stanford Advanced Materials, Inc., USA were used to fabricate rotors for the PoWER devices. Nickel-plated neodymium block magnets of dimensions 12.7 mm × 6.35 mm × 6.35 mm were purchased from K & J magnetics, Inc., USA. These permanent magnets were magnetized through their thickness and had a surface field strength of 5248 Gauss. An axial flux generator was built as it has low cogging torque. The details of the generator developed in this study are provided in the ESI.† As shown in the ESI,† Fig. S4, the axial flux electric generator used in the PoWER device had one stator and two rotors on either side of the stator. The stator consists of a set of eight teardrop shaped coils; each coil has copper wire of gauge size 42 AWG. Each of the generator rotors contains a set of eight arc shaped permanent magnets. All other components were 3D printed.

Measurement of electrical output and characteristics

The voltage generated by the PoWER devices was recorded using a National Instruments NI myDAQ. The angular speed was measured using a non-contact type optical digital Tachometer, DT-209X, by SHIMPO Instruments, USA. A resistance substitution box, RS-200W, by IET Labs, Inc. was used during resistance sweep experiments. Type T thermocouples were used to detect the temperature of the heat source. For calculating the electrical power, we have used the root mean square (rms) voltage. We first recorded continuous data for the rms voltage, which was obtained using consecutive data points for the instantaneous voltage. The arithmetic mean of the recorded rms voltage data was then used to calculate the average power, which is reported in Fig. 4a–d and Fig. 6a and b. The maximum and minimum values of the power shown in Fig. 3a–c were calculated based on the maximum rms voltage and the minimum rms voltage recorded during the resistance sweep experiments. The effect of wind on the performance of the PoWER devices was studied using a 0.7 m subsonic open jet wind tunnel. The magnetic characterization of the Gd sample was performed using the quantum design physical property measurement system (PPMS). The specific heat measurements were performed using differential scanning calorimetry (DSC).

Author contributions

R. A. K. and S. P. conceived the idea; B. D. and J. G. fabricated the electric generator; R. A. K, D. K., A. H., and A. M. performed the experiments; R. A. K., D. K. and D. M. prepared the demonstration videos. M. G. K and H. K. performed the magnetic characterization. A. N. performed the DSC measurements. S. P. supervised the research. All authors contributed to the discussion. R. A. K. and S. P. wrote the manuscript.

Conflicts of interest

There are no conflicts to declare.

Acknowledgements

The authors (R. A. K. and S. P.) gratefully acknowledge the financial support from the DARPA MATRIX program (ARO TE3). R. A. K. acknowledges the financial support from the ICTAS Doctoral Scholars Program. AN would like to acknowledge the financial support through ARO. MGK was supported through the Air Force Office of Scientific Research under award number ⟨FA9550-17-1-0341⟩. HBK would like to acknowledge the financial support through AMRDEC (membership of NSF I/UCRC: Center for Energy Harvesting Materials and Systems (CEHMS)). Undergraduate research students working on the program were supported from the Office of Naval Research through grant number N000141712520. We also thank senior design students: Jessica Hamilton and Ben Rice for their contribution through senior design projects.

References

1 C. Forman, I. K. Muritala, R. Pardemann and B. Meyer, *Renewable Sustainable Energy Rev.*, 2016, **57**, 1568–1579.
2 B.-T. Liu, K.-H. Chien and C.-C. Wang, *Energy*, 2004, **29**, 1207–1217.
3 B. Mohanty and G. Paloso, *Heat Recovery Syst. CHP*, 1992, **12**, 143–158.
4 A. Kalina and H. Leibowitz, *Trans. - Geotherm. Resour. Counc.*, 1989, **13**, 605–611.
5 E. Barbier, *Renewable Sustainable Energy Rev.*, 2002, **6**, 3–65.
6 H. M. Hettiarachchi, M. Golubovic, W. M. Worek and Y. Ikegami, *Energy*, 2007, **32**, 1698–1706.
7 J. Senft, *Mechanical efficiency considerations in the design of an ultra low temperature differential Stirling engine, Report 0148-7191, SAE Technical Paper*, 1992.

8 M. Y. Won and P. S. Jung, *Transactions of the Korean Society of Mechanical Engineers B*, 2005, **29**, 519–525.
9 K. Wang, S. R. Sanders, S. Dubey, F. H. Choo and F. Duan, *Renewable Sustainable Energy Rev.*, 2016, **62**, 89–108.
10 D. Thimsen, *Stirling Engine Assessment*, EPRI, Palo Alto, 2002, p. 1007317.
11 B. J. Kim, D. H. Kim, Y.-Y. Lee, H.-W. Shin, G. S. Han, J. S. Hong, K. Mahmood, T. K. Ahn, Y.-C. Joo and K. S. Hong, *Energy Environ. Sci.*, 2015, **8**, 916–921.
12 J. Yoon, A. J. Baca, S.-I. Park, P. Elvikis, J. B. Geddes III, L. Li, R. H. Kim, J. Xiao, S. Wang and T.-H. Kim, in *Materials for Sustainable Energy: A Collection of Peer-Reviewed Research and Review Articles from Nature Publishing Group*, World Scientific, 2011, pp. 38–46.
13 M.-L. Seol, J.-H. Woo, S.-B. Jeon, D. Kim, S.-J. Park, J. Hur and Y.-K. Choi, *Nano Energy*, 2015, **14**, 201–208.
14 Z. L. Wang, J. Chen and L. Lin, *Energy Environ. Sci.*, 2015, **8**, 2250–2282.
15 G. T. Hwang, M. Byun, C. K. Jeong and K. J. Lee, *Adv. Healthcare Mater.*, 2015, **4**, 646–658.
16 R. Kishore and S. Priya, *Materials*, 2018, **11**, 1433.
17 S. J. Kim, H. E. Lee, H. Choi, Y. Kim, J. H. We, J. S. Shin, K. J. Lee and B. J. Cho, *ACS Nano*, 2016, **10**, 10851–10857.
18 S. J. Kim, H. Choi, Y. Kim, J. H. We, J. S. Shin, H. E. Lee, M.-W. Oh, K. J. Lee and B. J. Cho, *Nano Energy*, 2017, **31**, 258–263.
19 X. Hu, P. Jood, M. Ohta, M. Kunii, K. Nagase, H. Nishiate, M. G. Kanatzidis and A. Yamamoto, *Energy Environ. Sci.*, 2016, **9**, 517–529.
20 A. Muto, J. Yang, B. Poudel, Z. Ren and G. Chen, *Adv. Energy Mater.*, 2013, **3**, 245–251.
21 C. B. Vining, *Nat. Mater.*, 2009, **8**, 83–85.
22 Y. Sato, N. Yoshida, Y. Tanabe, H. Fujita and N. Ooiwa, *Electr. Eng. Jpn*, 2008, **165**, 8–15.
23 D. Avirovik, R. A. Kishore, D. Vuckovic and S. Priya, *Energy Harvesting Systems*, 2014, **1**, 13–18.
24 Q. Leng, L. Chen, H. Guo, J. Liu, G. Liu, C. Hu and Y. Xi, *J. Mater. Chem. A*, 2014, **2**, 11940–11947.
25 S. H. Kim, M. D. Lima, M. E. Kozlov, C. S. Haines, G. M. Spinks, S. Aziz, C. Choi, H. J. Sim, X. Wang and H. Lu, *Energy Environ. Sci.*, 2015, **8**, 3336–3344.
26 T. A. Edison, *US Pat.*, 380100, 1888.
27 T. A. Edison, *US Pat.*, 476983, 1892.
28 N. Tesla, *US Pat.*, 396121, 1889.
29 N. Tesla, *US Pat.*, 428057, 1890.
30 J. Elliott, *J. Appl. Phys.*, 1959, **30**, 1774–1777.
31 R. A. Kishore and S. Priya, *Renewable Sustainable Energy Rev.*, 2018, **81**, 33–44.
32 L. D. Kirol and J. I. Mills, *J. Appl. Phys.*, 1984, **56**, 824–828.
33 D. Solomon, *J. Appl. Phys.*, 1988, **63**, 915–921.
34 D. Solomon, *J. Appl. Phys.*, 1989, **65**, 3687–3693.
35 D. Solomon, *Energy Convers. Manage.*, 1991, **31**, 157–173.
36 J. Chun, H.-C. Song, M.-G. Kang, H. B. Kang, R. A. Kishore and S. Priya, *Sci. Rep.*, 2017, **7**, 41383.
37 M. Ujihara, G. Carman and D. Lee, *Appl. Phys. Lett.*, 2007, **91**, 093508.
38 C.-C. Chen, T.-K. Chung, C.-Y. Tseng, C.-F. Hung, P.-C. Yeh and C.-C. Cheng, *IEEE Trans. Magn.*, 2015, **51**, 1–9.
39 L. Carlioz, J. Delamare and S. Basrour, 2009.
40 J. Chun, R. A. Kishore, P. Kumar, M.-G. Kang, H. B. Kang, M. Sanghadasa and S. Priya, *ACS Appl. Mater. Interfaces*, 2018, **10**, 10796–10803.
41 Gadolinium: http://mriquestions.com/why-gadolinium.html, accessed on 12/20/2018.
42 S. Y. Dan'Kov, A. Tishin, V. Pecharsky and K. Gschneidner, *Phys. Rev. B: Condens. Matter Mater. Phys.*, 1998, **57**, 3478.
43 J. Cable and E. Wollan, *Phys. Rev.*, 1968, **165**, 733.
44 A. Lindbaum and M. Rotter, Spontaneous Magnetoelastic Effects in Gadolinium Compounds, *Handbook of Magnetic Materials*, Elsevier, 2002, ch. 4, vol. 14, pp. 307–362.
45 A. Vaterlaus, T. Beutler and F. Meier, *Phys. Rev. Lett.*, 1991, **67**, 3314.
46 C. Glorieux, J. Thoen, G. Bednarz, M. A. White and D. Geldart, *Phys. Rev. B: Condens. Matter Mater. Phys.*, 1995, **52**, 12770.
47 H.-C. Song, D. Maurya, J. Chun, Y. Zhou, M.-E. Song, D. Gray, N. K. Yamoah, D. Kumar, A. McDannald and M. Jain, *Energy Harvesting Systems*, 2017, **4**, 57–65.
48 V. K. Pecharsky and K. A. Gschneidner Jr, *Appl. Phys. Lett.*, 1997, **70**, 3299–3301.
49 V. Pecharsky and K. Gschneidner Jr, *J. Magn. Magn. Mater.*, 1997, **167**, L179–L184.
50 F.-x. Hu, B.-g. Shen, J.-r. Sun and G.-h. Wu, *Phys. Rev. B: Condens. Matter Mater. Phys.*, 2001, **64**, 132412.
51 F.-x. Hu, B.-g. Shen and J.-r. Sun, *Appl. Phys. Lett.*, 2000, **76**, 3460–3462.

